



Printable anisotropic magnetoresistance sensors for highly compliant electronics

Eduardo Sergio Oliveros Mata¹ · Gilbert Santiago Cañón Bermúdez¹ · Minjeong Ha¹ · Tobias Kosub¹ · Yevhen Zabala² · Jürgen Fassbender¹ · Denys Makarov¹

Received: 11 September 2020 / Accepted: 2 March 2021 / Published online: 25 March 2021
© The Author(s) 2021

Abstract

Printed electronics are attractive due to their low-cost and large-area processing features, which have been successfully extended to magnetoresistive sensors and devices. Here, we introduce and characterize a new kind of magnetoresistive paste based on the anisotropic magnetoresistive (AMR) effect. The paste is a composite of 100-nm-thick permalloy/tantalum flakes embedded in an elastomer matrix, which promotes the formation of appropriately conductive percolation networks. Sensors printed with this paste showed stable magnetoresistive properties upon mechanical bending. The AMR value of this sensor is 0.34% in the field of 400 mT. Still, the response is stable and allows to resolve sub-mT field steps. When printed on ultra-thin 2.5- μm -thick Mylar foil, the sensor can be completely folded without losing magnetoresistive performance and mechanically withstand 20 μm bending radius. The developed compliant printed AMR sensor would be attractive to implement on curved and/or dynamic bendable surfaces for on-skin applications and interactive printed electronics.

Keywords Flexible sensor · Anisotropic magnetoresistance · Printed electronics

1 Introduction

Printing technologies are low-cost ubiquitous techniques that are in the manufacturing process of household goods and devices [1–5]. Apart from the impression of product labels or the printed version of this journal, printing is now being explored to obtain multifunctional electronic devices as RFID (radio-frequency identification) antennas [6], solar cells [7], ferroelectric memories [8], and magnetic field sensors [9]. To arrive to the widespread of printed systems, we need to address the main challenges of printable electronics which are related to the instability, noise, and the low conductivity of the inks or pastes [10, 11]. Overcoming these issues will allow us to produce on-demand functional parts with printed utility systems for diverse applications as implants [12], smart devices [13], and sensors [14].

Printed magnetic field sensors have been underrepresented, mainly due to the complexity to obtain printable, well-conductive magnetosensitive composites with stable resistance readout [9, 15]. The introduction of magnetic particles into elastomer matrices is one approach to obtain magnetoresponsive compounds [16–20]. Magnetic nanoparticles embedded in conductive agglomerates can be concatenated using an external magnetic field during the curing process of the binder (e.g. Polydimethylsiloxane (PDMS)) [17, 21, 22]. The resulting composite is a magnetoresistive compound that can measure the magnetic field components in the direction of the aligned particles [17]. After the development of these flexible magnetoresistive composites, examples of solution-processable magnetic sensors with gel-like binders and elastomers appeared [23]. These systems achieved large resistance change signal, yet typically at the expense of rather high resistance and noise. A paradigm change arrived with the fabrication of pastes that were not based on nanoparticles, but on magnetic flakes obtained from thin film deposition [24, 25]. Flakes-based GMR (Giant magnetoresistance) printed sensors have achieved 37% resistance change, with good temperature stability up to 95 °C, and flexed down

✉ Denys Makarov
d.makarov@hzdr.de

¹ Helmholtz-Zentrum Dresden - Rossendorf e.V., Institute of Ion Beam Physics and Materials Research, Bautzner Landstrasse 400, 01328 Dresden, Germany

² Institute of Nuclear Physics, Polish Academy of Sciences, 31342 Kraków, Poland

to 12 mm bending radii as a result of the incorporation of polymer binders like polyepichlorohydrin (PCH) [25].

By now, printed magnetoelectronics were based on GMR sensors [9, 24–26]. Although they provide a large magnetoresistive effect, this technology requires involved fabrication due to the necessity to control the thickness of individual layers down to sub-nm [27, 28]. In this regard, the use of AMR films is attractive because the complexity to obtain a magnetosensitive material is reduced [29, 30].

In this work, we fabricate and investigate the sensing performance of a printable sensor based on AMR flakes of permalloy (Py). We demonstrate that despite having a lower magnetoresistance than GMR sensors, the signal stability is enough to resolve sub-mT range fields. In addition, the obtained printable paste has low resistance, can be printed in ultrathin polymer foils (2.5 μm), and withstands mechanical deformations down to 20 mm bending radii which makes it attractive for bendable and compliant electronics for on-skin applications [30–33].

2 Methods

2.1 Fabrication of a compliant and printable AMR sensor

2.1.1 Preparation of AMR powder

A 4-inch Si/SiO₂ wafer was spin-coated with AZ1505 photoresist (Microchemicals GmbH, Germany) as a sacrificial layer. Then, a thin film of [Ta (5 nm)/Py (100 nm)] was deposited on top of the covered wafer by magnetron sputtering deposition at room temperature (deposition rate = 0.14/0.18 (Ta/Py) nm/s, base pressure = 1×10^{-7} mbar, Ar sputter pressure = 9×10^{-4} mbar). The flakes were formed after dissolving the photoresist in acetone bath with an ultrasound-assisted lift-off procedure. The Py/Ta flakes were then recovered with a permanent magnet and rinsed with isopropanol. The remaining solvent was evaporated in an oven at 70 °C for 1 h until a dry powder was obtained.

2.1.2 Paste formulation and printing

The Py/Ta powder was incorporated in poly(styrene-butadiene-styrene) copolymer (SBS). First, the SBS was dissolved in xylol to a 0.15 g/mL concentration with magnetic stirring for 8 h. Afterwards, the magnetic flakes were added until we achieved a concentration of 50 mg/mL in the SBS solution. The obtained paste is then printed by pipetting onto the desired substrate and dried for 2 h at room temperature.

2.1.3 Gold contacts fabrication on Mylar foil

Au contacts were fabricated using e-beam deposition with a custom designed shadow mask. 5 cm \times 5 cm pieces of 2.5 μm thick Mylar foils (Chemplex Industries Inc., USA) were attached to a polydimethylsiloxane-coated (PDMS, Sylgard 184, Dow Corning, USA) glass substrate. Vinyl foil (Oracal 751) patterned with a plotter cutter (Silhouette portrait) was attached on Mylar foils as shadow masks. After e-beam deposition of a [Ti (5 nm)/Au (50 nm)] layer (deposition rate = 0.05/0.2 (Ti/Au) nm/s, base pressure = 1×10^{-8} mbar), the shadow mask was removed to obtain the desired patterns.

2.2 Magnetoresistive and mechanical characterization

2.2.1 AMR characterization

The resistance was measured in a four-point configuration with a Tensormeter setup (HZDR Innovation, Germany) [34, 35]. The amplitude of the applied voltage in the external contacts was 200 mV to induce a current of around 10 mA flowing through the sensor. A computer-controlled electromagnet applied magnetic field sweeps in a ± 400 mT range. The AMR response of the sensor was calculated as $100\% \times (R(H) - R(H_{\text{sat}}))/R(H_{\text{sat}})$, where H_{sat} refers to the field when the resistance value saturates and H to each static field value.

2.2.2 Signal-to-noise analysis

The time evolution of the four-point resistance of the sensor was measured with a Tensormeter to determine the noise characteristics of the sensor. The four-point resistance in time was assessed with 5 ms integration time data points and then applying a Fast Fourier Transform (FFT) algorithm to obtain the noise spectral density of the signal.

2.2.3 AMR response upon bending

The sensor was mounted onto a bending setup to measure the AMR response at different bending radii. The bending setup allowed us to curve the sample to predefined fixed radius varying from flat state down to 2 mm. The magnetic field was applied in plane perpendicular to the bending axis. In this way, we ensure that the sensor was exposed to a homogeneous magnetic field of ± 300 mT during the experiment.

3 Results

3.1 Magnetoresistive performance of printed AMR sensors

Figure 1a shows a schematic representation of the fabrication process of the Py/Ta flakes. A wafer was spin coated with a sacrificial layer and deposited with a 105-nm-thick Py/Ta AMR film. The AMR performance was measured on as prepared samples, revealing an AMR ratio of 1.9% and a saturation field of 5 mT (Fig. 1b). Then, the thin layer of Py/Ta was particulated dissolving the sacrificial resist in acetone with ultrasound assistance. After solvent evaporation, a magnetosensitive powder consisting of Py/Ta flakes was obtained, and this powder mainly consists of

tubular flakes (Fig. 1c) with a log-normal distribution for length with $l_{\text{mean}} = 85 \mu\text{m}$ and width with $w_{\text{mean}} = 26 \mu\text{m}$ (Fig. 1d). At this stage, the AMR flakes conform a dry powder which is employed in subsequent processing steps as the solid phase of the magnetic composite.

The incorporation of a binder is necessary to promote both good contact between particles and conformal adhesion to a target surface. For printed flexible applications, it is necessary to choose an elastomer binder with low curing temperature and good adhesion properties. In this work, we use the SBS triblock copolymer since it promotes highly interconnected electrically conductive pathways which provide stable electrical signal even upon mechanical deformation [36]. Once the flakes are homogeneously incorporated into the SBS matrix, the resulting paste was applied with a pipette on a substrate (schematics

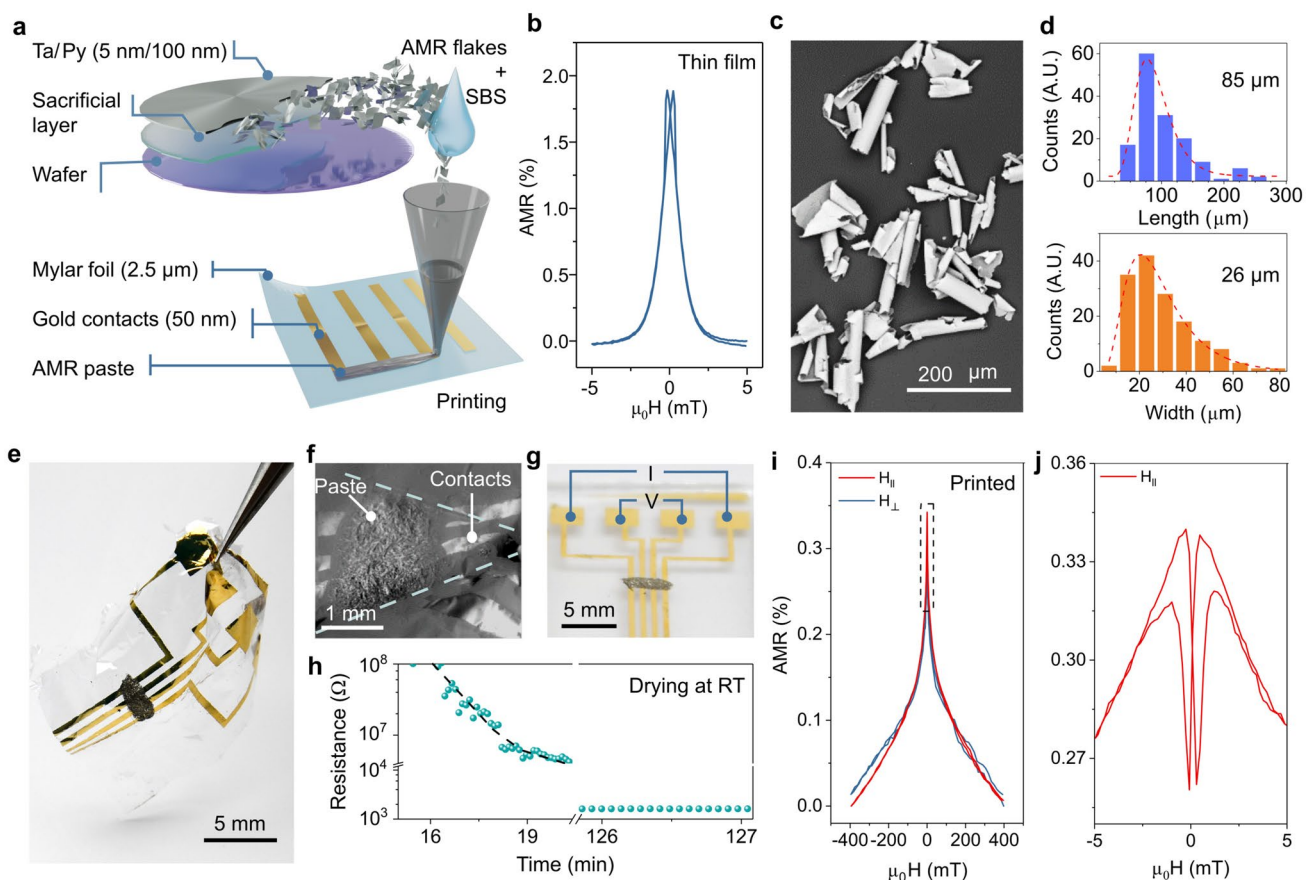


Fig. 1 **a** Fabrication steps of the printed AMR sensor. A magnetic paste is obtained from the mixture of Py/Ta flakes and SBS triblock copolymer. This solution is printed on ultrathin foils to obtain a highly compliant printed AMR sensor. **b** Reference AMR curve of the deposited Py/Ta film measured on the wafer. **c** SEM micrograph of the obtained Py/Ta flakes after dissolving the sacrificial layer. The flakes are mainly tubular shaped, with mean size $85 \mu\text{m} \times 26 \mu\text{m}$ as illustrated in the **d** histograms representing the length and width distribution. **e** Finished printed sensor on an ultrathin Mylar foil. **f**

The SEM micrograph shows that the sensor can comply to a highly irregular surface. **g** The changes in resistance produced by an external magnetic field are measured in a 4-point configuration. This layout allows measuring the **h** resistance during the drying process of the paste after printing, and the **i** AMR response of the sensor when an in-plane (parallel/perpendicular with respect to the current flow) magnetic field is applied. **j** Inset showing the AMR response at low fields $\pm 5 \text{ mT}$

in Fig. 1a). We used a Mylar foil ($2.5\ \mu\text{m}$) with patterned Au electrodes as a mechanically imperceptible flexible target substrate for printing (Fig. 1e). The ultrathin flexible Mylar substrate allows the sensor to fully comply to uneven surfaces with creases below 1 mm (Fig. 1f). To exclude the resistance contribution of the contacts from the sensing signal, the Au electrodes are patterned in a four-point configuration (Fig. 1g). After printing, we assessed the drying time necessary to have a stable sensor response. The paste started to show a measurable signal at 16 min (Fig. 1h). After 125 min, the paste resistance decreased five orders of magnitude and converge to a stable value. The resistance value stabilization was the sign that the solvent was completely evaporated.

To assess the AMR response of the printed sensor, we performed a magnetoresistive characterization (Fig. 1i). During the measurement, the field was applied in-plane parallel and perpendicular to the current direction to assess the anisotropic response of the sensor. In the parallel direction, the sensor demonstrated a 0.34% response; in the case when the applied field was perpendicular to the current flow direction, the AMR response was 0.28%. The sensor also demonstrated to have two different sensitivity regions, for magnetic flux densities above 5 mT the max slope was $12\% \text{ T}^{-1}$; meanwhile, the sensitivity reached $190\% \text{ T}^{-1}$ below 5 mT (Fig. 1j).

3.2 Bending performance

The bending properties are important to define the possibility to incorporate AMR printable sensors in, for instance, wearable applications. For this, the printed sensor was subjected to an analysis of its performance at different bending radii. We started with the sensor in flat layout and measured the AMR response upon bending, to predetermined radii of 6, 4, and 2 mm (Fig. 2a). During the experiment, the sensor showed a stable AMR response of around 0.28% (Fig. 2b).

A good percolation in a flakes system with a high number of interconnections allows to the network to compensate the connection breaks that may occur during the bending. In a system with sufficiently large amount of flakes, the current is able to pass through different paths in the network and maintain similar properties as the initial system. Despite having a relatively high concentration of conductive magnetoresistive flakes, the printed composite can withstand mechanically the bending up to $20\ \mu\text{m}$ bending radius (Fig. 2c) without any sign of flake delamination. The smart combination of thin foils and flexible materials allowed us to achieve this stable mechanical performance that demonstrate the attractiveness to use this ultrathin foils as a substrate for highly compliant printed sensors.

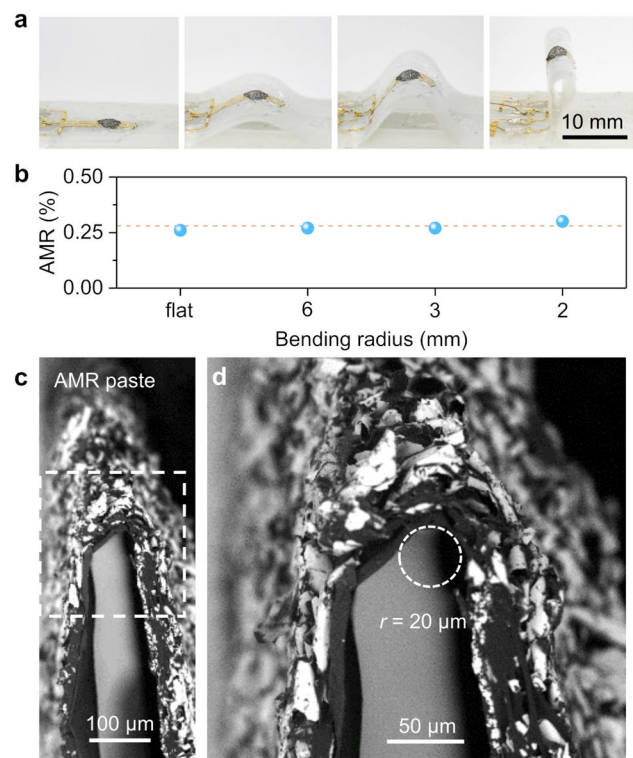


Fig. 2 **a** Photographs revealing the bending state of the sensor and **b** the respective AMR response measured at ± 400 mT. **c** SEM micrograph of the printed AMR sensor upon complete folding and **d** an inset showing good adhesion of the AMR flakes down to $20\ \mu\text{m}$ bending radius

3.3 Detection at low magnetic fields

The World Health Organization has established 40 mT as the safe continuous exposure limit for humans [37]. In this respect, the possibility to measure low fields is important to comply with this safety standard. To quantify the sensor performance, we first analyzed the stability of the resistance in time. We consider a window of 60 s to measure the resistance level variation of the magnetoresistive sensor without stimuli in time. When sampled at 60 S/s the four-point resistance of the sensor with nominal resistance of $R_0 = 25.693\ \Omega$ had a peak fluctuation of $\pm 2\ \text{m}\Omega$, this was consistent among different iterations, as shown in Fig. 3a. When applying FFT algorithm, the noise spectra of these signals (Fig. 3b) showed a $1/\sqrt{f}$ trend with noise density at 1 Hz, $n_{1\text{Hz}} = 6.1 \times 10^{-4}\ \Omega/\sqrt{\text{Hz}}$. Considering these parameters for a 3-sigma (3σ) confidence detection, the expected resolution of the sensor implementation is $60\ \mu\text{T}$ in the region of highest sensitivity. This confirms the capabilities of the sensor to differentiate sub-mT magnetic fields with high level of confidence. To confirm the high stability of the sensor, we tracked the sensor response from 0 up to only $300\ \mu\text{T}$. The sensor showed a linear trend with

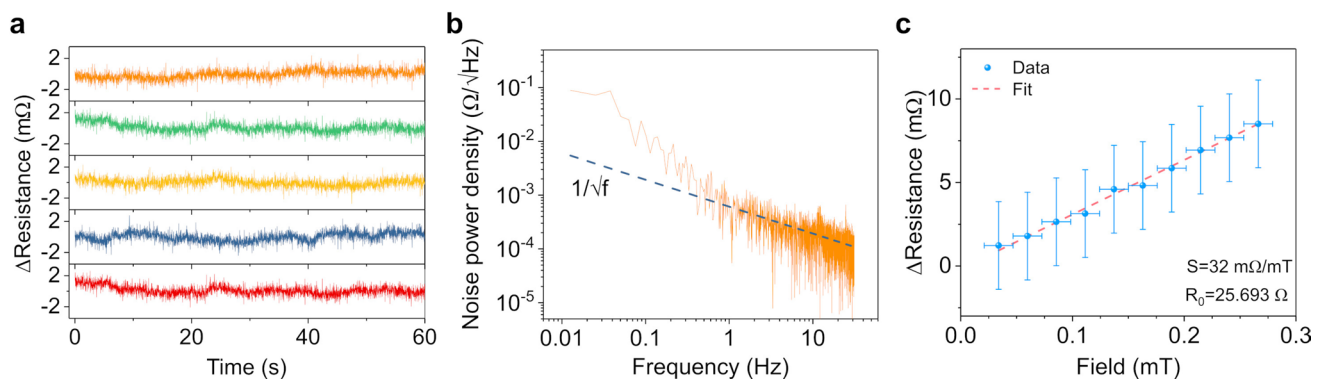


Fig. 3 **a** Resistance change in time of the printed AMR sensor. **b** Noise spectral density of the data shown in the top panel in **a**. **c** Linear response of the printed AMR sensor in sub-mT range

32 mΩ/mT sensitivity and the data distribution illustrated with 3-sigma error bars was in accordance with a sub-mT resolution (Fig. 3c).

3.4 Conclusions

Here, we report printable AMR sensors, which can be used to assess sub-mT fields and can be bent to 2 mm bending radius without sacrificing the sensor magnetoresistive performance. Also, we demonstrated the advantages of using SBS to prepare AMR-based sensors. The proposed formulation permits printing of sensors on ultrathin foils with stable mechanical performance even if the sensor is folded (20 μm bending radius). The equivalent floor noise of $n_1 \text{ Hz} = 6.1 \times 10^{-4} \text{ } \Omega / \sqrt{\text{Hz}}$ shown by the printed sensors allowed us to resolve fields below 1 mT which complies with the safety requirements of continuous magnetic field exposure from the WHO. The good performance at low fields and the high compliancy show the suitability to use this system for interactive wearable and printed electronics as switches, and sensors for physical activity. This technology can be also extended to additive manufacturing techniques, as 3D printing, for direct integration of magnetic sensors into on-demand functional parts.

Acknowledgements We thank Conrad Schubert, Rainer Kaltfen, and Dr. Jens Ingolf Mönch (all HZDR) for the deposition of metal films. Support by the Division of Process Technology and Devices, and Structural Characterization Facilities Rossendorf at the Ion Beam Center (IBC) at the HZDR is greatly appreciated. This work is financed via the German Research Foundation (DFG) Grants MA 5144/9-1, MA 5144/13-1, MA 5144/28-1, and Helmholtz Association of German Research Centres in the frame of the Helmholtz Innovation Lab FlexiSens.

Funding Open Access funding enabled and organized by Projekt DEAL.

Declarations

Conflict of interest The authors declare that they have no conflict of interest.

Open Access This article is licensed under a Creative Commons Attribution 4.0 International License, which permits use, sharing, adaptation, distribution and reproduction in any medium or format, as long as you give appropriate credit to the original author(s) and the source, provide a link to the Creative Commons licence, and indicate if changes were made. The images or other third party material in this article are included in the article's Creative Commons licence, unless indicated otherwise in a credit line to the material. If material is not included in the article's Creative Commons licence and your intended use is not permitted by statutory regulation or exceeds the permitted use, you will need to obtain permission directly from the copyright holder. To view a copy of this licence, visit <http://creativecommons.org/licenses/by/4.0/>.

References

1. Q. Huang, Y. Zhu, Printing conductive nanomaterials for flexible and stretchable electronics: a review of materials, processes, and applications. *Adv. Mater. Technol.* **4**(5), 1800546 (2019)
2. D. Tobjörk, R. Österbacka, Paper electronics. *Adv. Mater.* **23**(17), 1935 (2011)
3. T.D. Ngo, A. Kashani, G. Imbalzano, K.T. Nguyen, D. Hui, Additive manufacturing (3D printing): a review of materials, methods, applications and challenges. *Compos. B Eng.* **143**, 172 (2018)
4. J. Kim, R. Kumar, A.J. Bandodkar, J. Wang, Advanced materials for printed wearable electrochemical devices: a review. *Adv. Electron. Mater.* **3**(1), 1600260 (2017)
5. K. Fukuda, T. Someya, Recent progress in the development of printed thin-film transistors and circuits with high-resolution printing technology. *Adv. Mater.* **29**(25), 1602736 (2017)
6. L. Yang, A. Rida, R. Vyas, M.M. Tentzeris, RFID tag and RF structures on a paper substrate using inkjet-printing technology. *IEEE Trans. Microw. Theory Tech.* **55**(12), 2894 (2007)
7. S. Das, B. Yang, G. Gu, P.C. Joshi, I.N. Ivanov, C.M. Rouleau, T. Aytug, D.B. Geohegan, K. Xiao, High-performance flexible perovskite solar cells by using a combination of ultrasonic spray-coating and low thermal budget photonic curing. *ACS Photonics* **2**(6), 680 (2015)

8. S.J. Kang, Y.J. Park, I. Bae, K.J. Kim, H.C. Kim, S. Bauer, E.L. Thomas, C. Park, Printable ferroelectric PVDF/PMMA blend films with ultralow roughness for low voltage non-volatile polymer memory. *Adv. Funct. Mater.* **19**(17), 2812 (2009)
9. D. Makarov, D. Karnaushenko, O.G. Schmidt, Printable magnetoelectronics. *ChemPhysChem* **14**(9), 1771 (2013)
10. M. Singh, H.M. Haverinen, P. Dhagat, G.E. Jabbour, Inkjet printing process and its applications. *Adv. Mater.* **22**(6), 673 (2010)
11. E.B. Secor, P.L. Prabhurashi, K. Puntambekar, M.L. Geier, M.C. Hersam, Inkjet printing of high conductivity, flexible graphene patterns. *J. Phys. Chem. Lett.* **4**(8), 1347 (2013)
12. R. Feiner, T. Dvir, Tissue-electronics interfaces: from implantable devices to engineered tissues. *Nat. Rev. Mater.* **3**(1), 17076 (2017)
13. M.F. Farooqui, A. Shamim, Low cost inkjet printed smart bandage for wireless monitoring of chronic wounds. *Sci. Rep.* **6**, 28949 (2016)
14. Z. Chu, J. Peng, W. Jin, Advanced nanomaterial inks for screen-printed chemical sensors. *Sens. Actuators B Chem.* **243**, 919 (2017)
15. D. Makarov, M. Melzer, D. Karnaushenko, O.G. Schmidt, Shapeable magnetoelectronics. *Appl. Phys. Rev.* **3**(1), 011101 (2016)
16. Z. Varga, G. Filipcsei, M. Zrínyi, Smart composites with controlled anisotropy. *Polymer* **46**(18), 7779 (2005)
17. J.L. Mietta, P.I. Tamborenea, R.M. Negri, Anisotropic magnetoresistivity in structured elastomer composites: modelling and experiments. *Soft Matter* **12**(30), 6430 (2016)
18. L. Ding, S. Xuan, L. Pei, S. Wang, T. Hu, S. Zhang, X. Gong, Stress and magnetic field bimode detection sensors based on flexible CI/CNTS-PDMS sponges. *ACS Appl. Mater. Interfaces* **10**(36), 30774 (2018)
19. S. Sasaki, Y. Tsujiei, M. Kawai, T. Mitsumata, Electric conductivity and dielectric-breakdown behavior for polyurethane magnetic elastomers. *J. Phys. Chem. B* **121**(7), 1740 (2017)
20. L. Ding, Y. Wang, C. Sun, Q. Shu, T. Hu, S. Xuan, X. Gong, Three-dimensional structured dual-mode flexible sensors for highly sensitive tactile perception and noncontact sensing. *ACS Appl. Mater. Interfaces* **12**(18), 20955 (2020)
21. J.L. Mietta, M.M. Ruiz, P.S. Antonel, O.E. Perez, A. Butera, G. Jorge, R.M. Negri, Anisotropic magnetoresistance and piezoresistivity in structured Fe₃O₄-silver particles in PDMS elastomers at room temperature. *Langmuir* **28**(17), 6985 (2012)
22. Y. Bi, X. Zhang, G. Chen, J. Liu, J. Tang, W. Wang, Effect of polymer matrix elasticity on the magnetocapacitance characteristics for Fe₃O₄/PDMS nanocomposites: FEM modelling and experiment. *Mater. Res. Express* **6**(2), 025010 (2018)
23. J. Meyer, T. Rempel, M. Schäfers, F. Wittbracht, C. Müller, A. Patel, A. Hütten, Giant magnetoresistance effects in gel-like matrices. *Smart Mater. Struct.* **22**(2), 025032 (2013)
24. D. Karnaushenko, D. Makarov, C. Yan, R. Streubel, O.G. Schmidt, Printable giant magnetoresistive devices. *Adv. Mater.* **24**(33), 4518 (2012)
25. D. Karnaushenko, D. Makarov, M. Stöber, D.D. Karnaushenko, S. Baunack, O.G. Schmidt, High-performance magnetic sensorics for printable and flexible electronics. *Adv. Mater.* **27**(5), 880 (2015)
26. B. Cox, D. Davis, N. Crews, Creating magnetic field sensors from GMR nanowire networks. *Sens. Actuator A Phys.* **203**, 335 (2013)
27. D. Mosca, F. Petroff, A. Fert, P. Schroeder, W. Pratt Jr., R. Laloe, Oscillatory interlayer coupling and giant magnetoresistance in Co/Cu multilayers. *J. Magn. Magn. Mater.* **94**(1–2), L1 (1991)
28. S. Parkin, Giant magnetoresistance in magnetic nanostructures. *Annu. Rev. Mater. Sci.* **25**(1), 357 (1995)
29. P. Dimitrova, S. Andreev, L. Popova, Thin film integrated AMR sensor for linear position measurements. *Sens. Actuator A Phys.* **147**(2), 387 (2008)
30. G.S. Cañón Bermúdez, H. Fuchs, L. Bischoff, J. Fassbender, D. Makarov, Electronic-skin compasses for geomagnetic field-driven artificial magnetoreception and interactive electronics. *Nat. Electron.* **1**(11), 589 (2018)
31. M. Melzer, M. Kaltenbrunner, D. Makarov, D. Karnaushenko, D. Karnaushenko, T. Sekitani, T. Someya, O.G. Schmidt, Imperceptible magnetoelectronics. *Nat. Commun.* **6**(1), 6080 (2015)
32. G.S. Cañón Bermúdez, D.D. Karnaushenko, D. Karnaushenko, A. Lebanov, L. Bischoff, M. Kaltenbrunner, J. Fassbender, O.G. Schmidt, D. Makarov, Magnetosensitive e-skins with directional perception for augmented reality. *Sci. Adv.* **4**(1), eaao2623 (2018)
33. J. Ge, X. Wang, M. Drack, O. Volkov, M. Liang, G.S. Cañón-Bermúdez, R. Illing, C. Wang, S. Zhou, J. Fassbender et al., A bimodal soft electronic skin for tactile and touchless interaction in real time. *Nat. Commun.* **10**(1), 4405 (2019)
34. T. Kosub, M. Kopte, F. Radu, O.G. Schmidt, D. Makarov, All-electric access to the magnetic-field-invariant magnetization of antiferromagnets. *Phys. Rev. Lett.* **115**(9), 097201 (2015)
35. Tensormeter. <https://www.tensormeter.de/>
36. I. You, M. Kong, U. Jeong, Block copolymer elastomers for stretchable electronics. *Acc. Chem. Res.* **52**(1), 63 (2018)
37. World Health Organization, *Static Fields* (World Health Organization, Geneva, 2006).

Publisher's Note Springer Nature remains neutral with regard to jurisdictional claims in published maps and institutional affiliations.